Supporting Information:

Controlled doping of carbon nanotubes with metallocenes for application in hybrid carbon nanotube/Si solar cells

Xiaokai Li,[1] Louise M. Guard,[2] Jie Jiang,[3] Kelsey Sakimoto,[1] Jing-Shun Huang,[1] Jianguo Wu,[2] Jinyang Li,[1] Ravi Pokhrel,[2] Lianqing Yu,[1] Gary W. Brudvig,[2] Sohrab Ismail-Beigi,[3] Nilay Hazari,[2] and André D. Taylor[1]

[1]Department of Chemical and Environmental Engineering, Yale University, New Haven, Connecticut, 06511, USA

[2]Department of Chemistry, Yale University, New Haven, Connecticut, 06511, USA

[3]Department of Applied Physics, Yale University, New Haven, Connecticut, 06520, USA

E-mail: nilay.hazari@yale.edu or andre.taylor@yale.edu

I. Materials and methods

SWNT thin film fabrication methods: Superacid slide coating method: 3mL of degassed chlorosulfonic acid (Fluka, purum 98%) was added to 14 mg of single walled carbon nanotube (SWNT) (kindly supplied by SouthWest NanoTechnologies) and stirred vigorously for 3 days, inside a glove box filled with nitrogen. A drop of the prepared SWNT ink was sandwiched between two glass slides. The slides were manually pressed together until the desired film thickness was achieved (typically 30 to 50 nm). The two slides were then rapidly

slid across each other in opposite directions, producing a SWNT film on each glass slide. Each slide was either dried slowly inside a glove box or gently dipped into deionized water to remove any acid that had leached out of the film. The resulting film was floated on the top of deionized water to facilitate transfer to another substrate.

II. Supplementary figures and tables

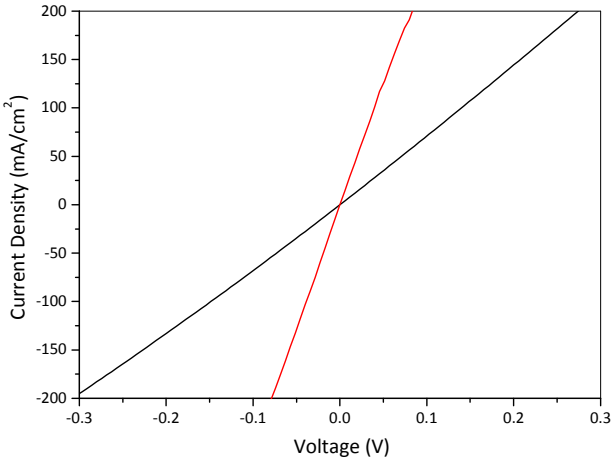

Figure S1. *J-V* characteristics of superacid sliding method made SWNT thin films on *p*-Si in the dark (black) and under 1 sun (AM1.5) illumination (red).

Table S1. Summary of the photovoltaic characteristics of *p*-SWNT/*n*-Si solar cells.

***p*-type dopants**	**Efficiency (%)**	**V_{oc} (V)**	**J_{sc} (mA/cm^2)**	***FF***
After current stimulation	0	0	0	0
$Cp_2Ti(PFBS)_2$	2.44	0.368	18.7	0.356
$Cp_2V(PFBS)_2$	6.00	0.474	23.9	0.529

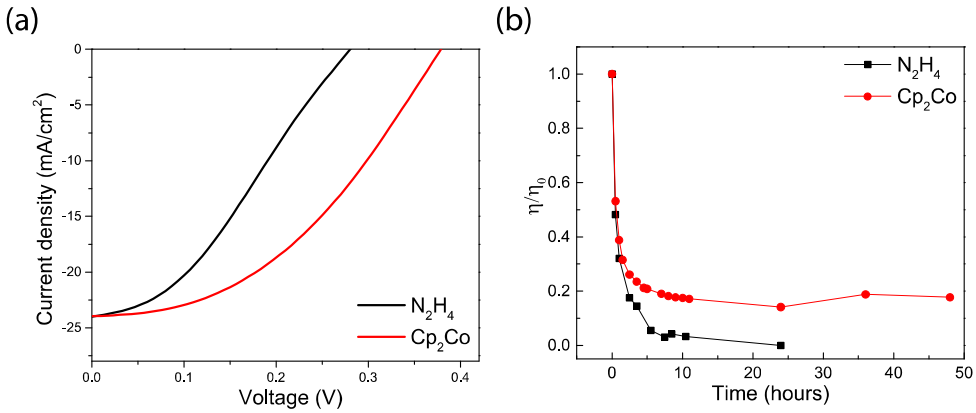

Figure S2. Comparison of the (a) *JV* characteristics and (b) stability of N_2H_4 and Cp_2Co doped *n*-SWNT/*p*-Si devices.

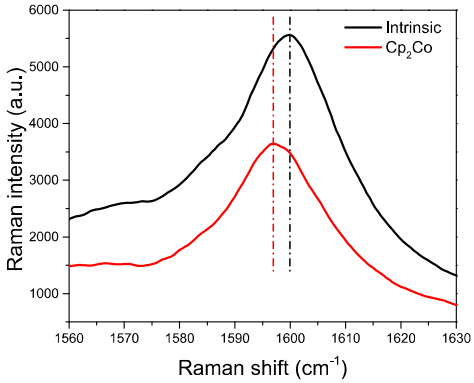

Figure S3. Raman spectra of G bands for (black) intrinsic and (red) Cp_2Co doped thin SWNT films

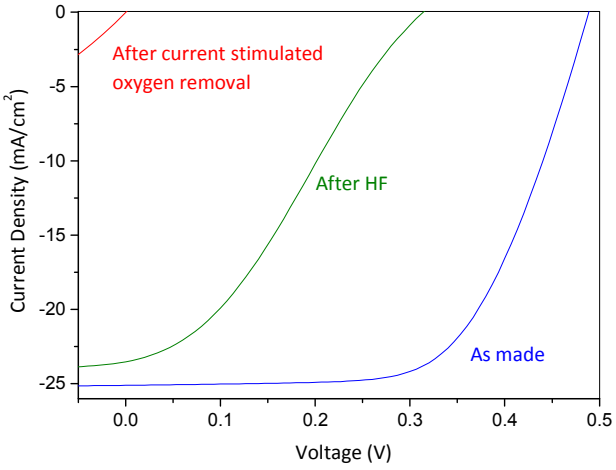

Figure S4. *J-V* characteristics of superacid sliding method made SWNT thin films on *n*-Si (blue), the *J-V* characteristics of the same device after HF vapor treatment (green) and the *J-V* characteristics of the same device after current stimulated oxygen removal (red) under 1 sun (AM1.5) illumination.

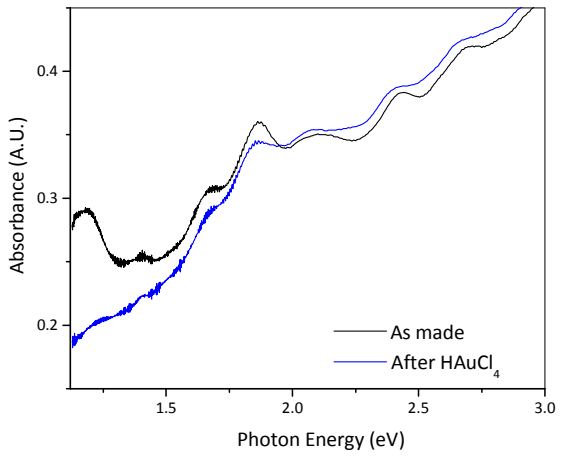

Figure S5. Reduction of the S_{22} absorption in SWNT after $HAuCl_4$ treatment.

III. Density Functional Theory Calculation of Metallocenes and Related Molecules

We use first principles theory to gain insight into the doping of carbon nanotubes by various metallocene complexes. The theoretical results allow us to find the effect of changing the metal center and ligands on the electronic structure of the molecules, which are used for *n*-type and *p*-type doping of the nanotubes. We employ density functional theory (DFT)[1] the plane wave supercell approach[2] with ultrasoft pseudopotentials[3] and the generalized gradient approximation for exchange and correlation.[4] From the calculations, our main extracted observables are the energies of the highest occupied molecular orbital (HOMO) and the lowest unoccupied molecular orbital (LUMO) with respect to vacuum. We expect that higher (less stable) HOMO energies make donation of electrons from HOMO to nanotube more likely and lead to more *n*-type doping, and the converse for the LUMO for which a lower energy should lead to enhanced p-type doping. Since hydrazine and nitric acid are well-known n-type and *p*-type dopants to carbon nanotubes, the HOMO of hydrazine is taken as a reference for the HOMO/SOMO of *n*-type dopants and the LUMO of nitric acid is taken as

the reference for the LUMO of *p*-type dopants. The supercell calculations employ a large unit cell where a single molecule is placed and surrounded by vacuum. Due to the periodic boundary conditions, the zero point of the potential is undefined, so that extracting HOMO and LUMO energies with respect to the vacuum requires some additional processing. As has been demonstrated previously,[5] DFT energy eigenvalues for isolated molecules have a linear behavior versus inverse volume for large super cells. Therefore, by running a few calculations in cubic supercells with sides of 10, 20, and 30 Å, we can fit the results by a straight line versus inverse volume and extrapolate to infinite volume. Figure S4 shows this procedure for the case of Cp_2Ni. We expect Cp_2Ni, $(C_6H_6)_2Cr$ and Cp_2Co should be *n*-type dopants. The calculated HOMO levels in Figure 4a of the main text are 2.58, 3.37, and 3.44 eV for Cp_2Ni, $(C_6H_6)_2Cr$ and Cp_2Co, respectively with respect to HOMO level of hydrazine. The trend of doping ability is generally consistent with that by experiment (Figure 4b). Figure S5 shows the electron wave function of the HOMO state for Cp_2Ni: the HOMO has significant weight on the metal center atom and thus changing this atom should change the HOMO energy.

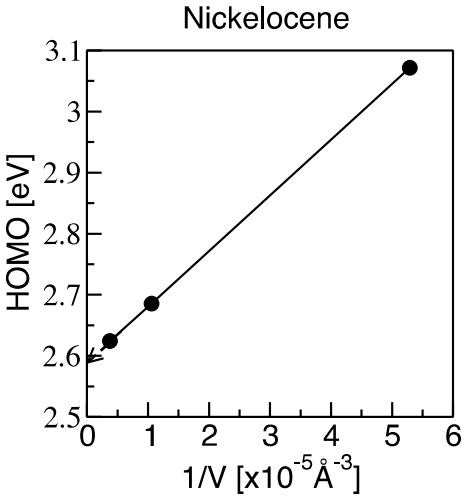

Figure S6. DFT calculated HOMO for Cp_2Ni as a function of inverse of supercell volume. The three points correspond to cubic supercells with sides of 10 20, and 30 Å, respectively. The extrapolated HOMO level is 2.58 eV below vacuum at infinite volume. (The vertical axis represents negative of the computed HOMO energy.)

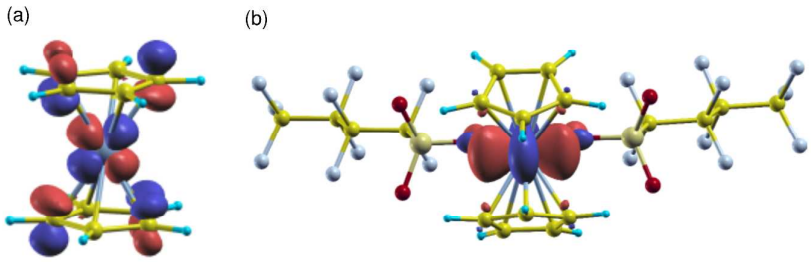

Figure S7. The wave functions for (a) HOMO of Cp_2Co and (b) partially occupied level of $Cp_2V(PFBS)_2$ visualized as isosurfaces. Red is for positive values and blue is for negative values.

On the other hand, titanocene with two perfluorobutanesulfonate ligands, $Cp_2Ti(PFBS)_2$, and its vanadium analogue, $Cp_2V(PFBS)_2$, are expected to be *p*-type dopants. The calculated LUMO levels in Figure 5b of the main text are -1.10 and -1.87 eV, respectively. $Cp_2V(PFBS)_2$ is predicted to be a better *p*-dopant than $Cp_2Ti(PFBS)_2$, which is confirmed by the experiment. The LUMO or partially filled level for these molecules are highly localized on the metal center as shown in Figure S5 for the case of $Cp_2V(PFBS)_2$.

IV. Experimental Procedures for the Preparation of Metallocenes and Related Molecules

General Methods

Experiments were performed under a dinitrogen atmosphere in an M-Braun dry box or using standard Schlenk techniques, unless otherwise noted. Under standard glovebox conditions, purging was not performed between uses of pentane, diethyl ether, benzene, toluene and THF; thus, when any of these solvents were used, traces of all these solvents were in the atmosphere and could be found intermixed in the solvent bottles. Moisture- and air-sensitive liquids were transferred by stainless steel cannula on a Schlenk line or in a dry box. Solvents were dried by passage through a column of activated alumina followed by storage under dinitrogen. All commercial chemicals were used as received, except where noted. Cp_2TiCl_2 was purchased from Acros Organics, Cp_2Co from Sigma Aldrich, Cp_2Ni from Alfa Aesar and

Cp_2VCl_2 and $(C_6H_6)_2Cr$ from Strem. Elemental analysis was performed by Robertson Microlit Laboratories. IR spectra were measured using a diamond smart orbit ATR on a Nicolet 6700 FT-IR instrument. Solution magnetic susceptibilities were determined by ^1H NMR spectroscopy using the Evans' method.[6] Literature procedures were utilized to synthesize Ag(PFBS).[7]

Synthesis and Characterization of Compounds

$Cp_2Ti(PFBS)_2$

$Cp_2Ti(PFBS)_2$ was prepared using literature methods.[8] X-ray diffraction quality crystals were grown by slow diffusion of pentane onto a saturated solution of dichloromethane. The X-ray structure is shown below.

$Cp_2V(PFBS)_2$

Ag(PFBS) (646 mg, 1.60 mmol) was dissolved in 15 ml THF and added to a suspension of Cp_2VCl_2 (200 mg, 0.80 mmol) in 20 ml THF. The mixture was stirred in the dark for 17 hours. The AgCl was removed by filtration and the resulting green solution evaporated to dryness to give a green powder. Recrystallization by layering diethyl ether onto a saturated THF solution of crude $Cp_2V(PFBS)_2$ at -30ºC yielded analytically pure $Cp_2V(PFBS)_2$ as a green micro-crystalline solid. Yield: 0.47 g (75%).

IR (ATR, Smart Orbit diamond plate, cm^{-1}): 3123.4, 2955.6, 1436.2, 1355.0, 1332.9, 1219.1, 1196.8, 1133.1, 1052.4, 1012.6, 840.3, 802.4, 737.4, 700.1, 652.6, 593.4, 775.0, 528.6. Anal. Calcd (found) for $C_{18}H_{10}F_{18}O_6S_2V$: C, 27.74 (27.49); H, 1.29 (1.51); N, 0.00 (<0.02). Magnetic susceptibility (THF): 1.76(5) μ_B.

In addition $Cp_2V(PFBS)_2$ was characterized by EPR spectroscopy. The X-band EPR spectrum displays (Figure S6) an axial g-profile ($g_1 = g_2 = 1.983$, $g_3 = 1.935$), consistent with one unpaired electron, and rhombic hyperfine coupling tensors (245, 150 and 363 MHz respectively).

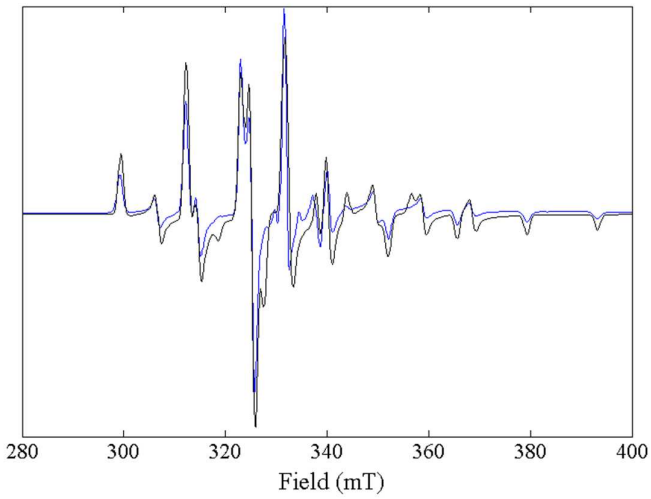

Figure S8. X-band EPR spectrum of **2** (blue) in 2-methyl THF at 7K and the corresponding simulation (black). The g-values from the simulation are $g_1 = 1.983$, $g_2 = 1.983$ and $g_3 = 1.935$.

The above X-band EPR spectrum was acquired on a Bruker ELEXSYS E500 EPR spectrometer equipped with a SHQ resonator and an Oxford ESR-900 helium-flow cryostat. EPR scans were acquired at 7 K with the following instrumental parameters: microwave frequency 9.39 GHz, microwave power 0.1 mW, modulation frequency 100 kHz, modulation amplitude 5 G, time constant 40.96 ms, conversion time 81.92 ms, center field 3450 G, and sweep width 2000 G. Simulations of the EPR spectrum was done using MATLAB 7.8 software and the EasySpin 4.0.0 package. An isotropic Gaussian broadening of 1 mT was used for the simulation.

X-ray Crystallography for $Cp_2Ti(PFBS)$

X-ray diffraction experiments were carried out on a Rigaku MicroMax-007HF diffractometer coupled to a Saturn994+ CCD detector with Cu Kα radiation (λ = 1.54178Å) at -180ºC. The crystals were mounted on MiTeGen polyimide loops with immersion oil. The data frames were processed using Rigaku CrystalClear and corrected for Lorentz and polarization effects. The structure was solved with the XS[9] structure solution program using direct methods and refined with the XL[9] refinement package using least squares minimisation. The non-hydrogen atoms were refined anisotropically. Hydrogen atoms were refined using the riding model. Details of the crystal and refinement data for $Cp_2Ti(PFBS)_2$ are given below and the structure is shown in Figure S7. The X-ray structure of $Cp_2Ti(PFBS)_2$ has been deposited in the Cambridge Crystallographic Data Centre (CCDC) (CCDC 980097).

In the solid state $Cp_2Ti(PFBS)_2$ exhibits a distorted tetrahedral geometry, typical of bent metallocenes,[10-13] where the O-Ti-Cp (where Cp represents the centroid of the Cp ring) angles range from 103.65-110.02º, Cp-Ti-Cp is 131.36º and O(21)-Ti(1)-O11 is 90.2(1)º. Within crystallographic error the Ti-O bonds are equal in length (2.015(3) and 2.046(3)Å), while the Ti-C bond distances are consistent with those observed in related complexes.[10, 12, 13]

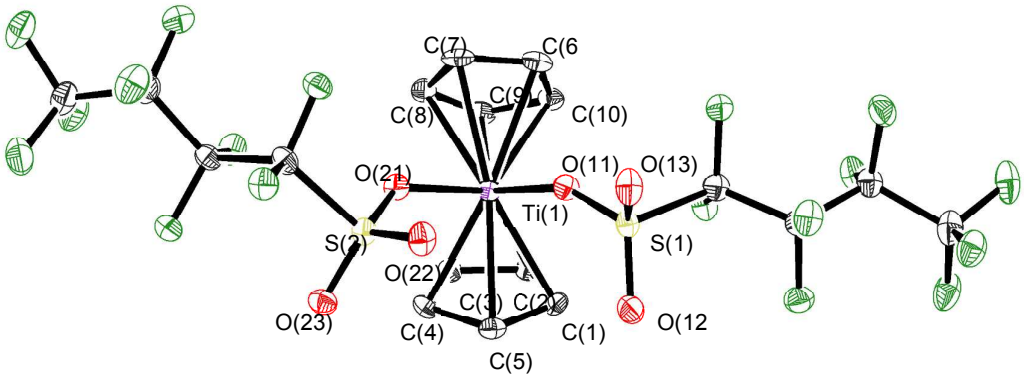

Figure S9. ORTEP[14] of $Cp_2Ti(PFBS)_2$ at 30% probability (hydrogen atoms have been omitted for clarity; Selected bond lengths (Å) and angles (°)): Ti(1)-C(1) 2.375(4), Ti(1)-C(2) 2.365(4), Ti(1)-C(3) 2.341(4), Ti(1)-C(4) 2.387(4), Ti(1)-C(5) 2.295(4), Ti(1)-C(6) 2.398(5), Ti(1)-C(7) 2.378(4), Ti(1)-C(8) 2.347(5), Ti(1)-C(9) 2.373(4), Ti(1)-C(10) 2.364(5), Ti(1)-O(11) 2.015(3), Ti(1)-O(21) 2.046(3), Ti(1)-O(11)-S(1) 153.0(2), Ti(1)-O(21)-S(2) 138.98(17).

Table S2. Crystal data and structure refinement for $Cp_2Ti(PFBS)_2$.

Empirical formula	$C_{18}\ H_{10}\ F_{18}\ O_6\ S_2\ Ti$	
Formula weight	776.28	
Temperature	93(2) K	
Wavelength	1.54187 Å	
Crystal system	Monoclinic	
Space group	*Ia*	
Unit cell dimensions	a = 12.5858(8) Å	α = 90°.
	b = 8.1766(3) Å	β = 103.779(7) °.
	c = 25.3415(17) Å	γ = 90 °.
Volume	2532.8(3) $Å^3$	
Z	4	
Density (calculated)	2.036 Mg/m^3	
Absorption coefficient	6.041 mm^{-1}	
F(000)	1528	
Crystal size	0.10 x 0.10 x 0.05 mm^3	
Theta range for data collection	3.59 to 66.07°.	
Index ranges	$-14 \le h \le 14, -9 \le k \le 9, -30 \le l \le 29$	
Reflections collected	37270	
Independent reflections	4337 [R(int) = 0.1105]	
Completeness to theta = 66.07°	99.2 %	
Absorption correction	Semi-empirical from equivalents	
Max. and min. transmission	0.7521 and 0.5833	
Refinement method	Full-matrix least-squares on F^2	
Data / restraints / parameters	4337 / 2 / 407	
Goodness-of-fit on F^2	1.092	
Final R indices [I>2sigma(I)]	R1 = 0.0408, wR2 = 0.1040	
R indices (all data)	R1 = 0.0426, wR2 = 0.1055	
Absolute structure parameter	0.476(8)	
Largest diff. peak and hole	0.563 and -0.349 e.$Å^{-3}$	

Table S3. Atomic coordinates (x 10^4) and equivalent isotropic displacement parameters ($Å^2$ x 10^3) for $Cp_2Ti(PFBS)_2$. U(eq) is defined as one third of the trace of the orthogonalized U^{ij} tensor.

	x	y	z	U(eq)
Ti(1)	5942(1)	7502(1)	2607(1)	23(1)
C(1)	7709(3)	7891(5)	3184(2)	31(1)
C(2)	7300(3)	9433(5)	2998(2)	30(1)
C(3)	7169(3)	9453(5)	2426(2)	29(1)
C(4)	7527(3)	7948(5)	2264(2)	29(1)
C(5)	7857(3)	6964(5)	2735(2)	32(1)
C(6)	4212(4)	7757(5)	2841(2)	33(1)
C(7)	4009(3)	7621(5)	2280(2)	35(1)
C(8)	4475(4)	9002(5)	2083(2)	34(1)
C(9)	4943(4)	9987(5)	2528(2)	34(1)
C(10)	4831(4)	9211(5)	3004(2)	32(1)
O(11)	5897(3)	5568(3)	3094(1)	32(1)
S(1)	6418(1)	4323(1)	3504(1)	30(1)
O(12)	7586(3)	4256(4)	3595(1)	40(1)
O(13)	5812(3)	2830(3)	3435(1)	42(1)
C(11)	6143(4)	5323(5)	4113(2)	33(1)
F(11)	6473(2)	6915(3)	4113(1)	40(1)
F(12)	5053(2)	5327(3)	4068(1)	43(1)
C(12)	6717(4)	4583(5)	4668(2)	31(1)
F(13)	7802(2)	4838(3)	4754(1)	42(1)
F(14)	6537(2)	2949(3)	4647(1)	42(1)
C(13)	6344(4)	5277(5)	5159(2)	34(1)
F(15)	6312(2)	6926(3)	5134(1)	42(1)
F(16)	5337(2)	4722(3)	5148(1)	46(1)
C(14)	7083(4)	4840(6)	5724(2)	45(1)
F(17)	7253(2)	3236(3)	5777(1)	49(1)
F(18)	6584(3)	5320(4)	6111(1)	56(1)
F(19)	8033(3)	5593(4)	5813(1)	57(1)
S(2)	6084(1)	4506(1)	1748(1)	29(1)
O(21)	5627(2)	5997(3)	1943(1)	30(1)
O(22)	6186(3)	3176(3)	2125(1)	39(1)
O(23)	7001(2)	4834(4)	1525(1)	35(1)
C(21)	4958(4)	3916(5)	1165(2)	32(1)
F(21)	5137(2)	2348(3)	1050(1)	38(1)
F(22)	4012(2)	3978(3)	1324(1)	37(1)
C(22)	4839(4)	4951(5)	646(2)	30(1)
F(23)	5720(2)	4660(3)	437(1)	39(1)
F(24)	4852(2)	6554(3)	785(1)	39(1)
C(23)	3795(4)	4631(5)	191(2)	37(1)
F(25)	3649(3)	2995(3)	123(1)	51(1)
F(26)	2927(2)	5256(4)	339(1)	52(1)
C(24)	3806(4)	5317(6)	-369(2)	44(1)
F(27)	4060(3)	6916(4)	-339(1)	56(1)
F(28)	2798(3)	5175(4)	-704(1)	56(1)
F(29)	4487(3)	4549(4)	-600(1)	64(1)

Table S4. Bond lengths [Å] and angles [°] for $Cp_2Ti(PFBS)_2$.

Ti(1)-O(11)	2.016(3)
Ti(1)-O(21)	2.046(3)
Ti(1)-C(3)	2.341(4)
Ti(1)-C(8)	2.347(4)
Ti(1)-C(10)	2.364(4)
Ti(1)-C(2)	2.365(4)
Ti(1)-C(9)	2.373(4)
Ti(1)-C(1)	2.375(4)
Ti(1)-C(7)	2.378(4)
Ti(1)-C(4)	2.386(4)
Ti(1)-C(5)	2.396(4)
Ti(1)-C(6)	2.397(4)
C(1)-C(2)	1.401(6)
C(1)-C(5)	1.417(6)
C(1)-H(1)	0.9500
C(2)-C(3)	1.420(6)
C(2)-H(2)	0.9500
C(3)-C(4)	1.405(6)
C(3)-H(3)	0.9500
C(4)-C(5)	1.418(6)
C(4)-H(4)	0.9500
C(5)-H(5)	0.9500
C(6)-C(7)	1.387(7)
C(6)-C(10)	1.427(6)
C(6)-H(6)	0.9500
C(7)-C(8)	1.418(6)
C(7)-H(7)	0.9500
C(8)-C(9)	1.397(6)
C(8)-H(8)	0.9500
C(9)-C(10)	1.399(6)
C(9)-H(9)	0.9500
C(10)-H(10)	0.9500
O(11)-S(1)	1.490(3)
S(1)-O(13)	1.428(3)
S(1)-O(12)	1.434(3)
S(1)-C(11)	1.850(5)
C(11)-F(12)	1.349(5)
C(11)-F(11)	1.366(5)
C(11)-C(12)	1.544(6)
C(12)-F(13)	1.346(5)
C(12)-F(14)	1.354(4)
C(12)-C(13)	1.538(6)
C(13)-F(16)	1.340(5)
C(13)-F(15)	1.350(5)
C(13)-C(14)	1.554(6)
C(14)-F(19)	1.316(6)
C(14)-F(17)	1.330(6)
C(14)-F(18)	1.341(6)
S(2)-O(23)	1.426(3)
S(2)-O(22)	1.434(3)
S(2)-O(21)	1.482(3)
S(2)-C(21)	1.850(5)
C(21)-F(21)	1.345(4)
C(21)-F(22)	1.346(5)
C(21)-C(22)	1.542(6)
C(22)-F(24)	1.356(5)
C(22)-F(23)	1.359(5)
C(22)-C(23)	1.549(6)
C(23)-F(26)	1.338(5)

C(23)-F(25)	1.356(5)
C(23)-C(24)	1.530(7)
C(24)-F(29)	1.308(6)
C(24)-F(27)	1.344(6)
C(24)-F(28)	1.353(6)

O(11)-Ti(1)-O(21)	90.24(11)
O(11)-Ti(1)-C(3)	140.45(15)
O(21)-Ti(1)-C(3)	104.84(13)
O(11)-Ti(1)-C(8)	128.61(15)
O(21)-Ti(1)-C(8)	82.91(13)
C(3)-Ti(1)-C(8)	89.95(15)
O(11)-Ti(1)-C(10)	95.59(14)
O(21)-Ti(1)-C(10)	133.41(14)
C(3)-Ti(1)-C(10)	99.50(15)
C(8)-Ti(1)-C(10)	57.78(15)
O(11)-Ti(1)-C(2)	112.97(14)
O(21)-Ti(1)-C(2)	136.51(13)
C(3)-Ti(1)-C(2)	35.13(15)
C(8)-Ti(1)-C(2)	106.28(15)
C(10)-Ti(1)-C(2)	82.44(15)
O(11)-Ti(1)-C(9)	129.20(14)
O(21)-Ti(1)-C(9)	116.80(14)
C(3)-Ti(1)-C(9)	76.15(15)
C(8)-Ti(1)-C(9)	34.44(16)
C(10)-Ti(1)-C(9)	34.36(15)
C(2)-Ti(1)-C(9)	77.21(16)
O(11)-Ti(1)-C(1)	83.48(14)
O(21)-Ti(1)-C(1)	123.87(14)
C(3)-Ti(1)-C(1)	57.63(14)
C(8)-Ti(1)-C(1)	140.66(16)
C(10)-Ti(1)-C(1)	102.72(16)
C(2)-Ti(1)-C(1)	34.38(15)
C(9)-Ti(1)-C(1)	109.66(16)
O(11)-Ti(1)-C(7)	94.03(15)
O(21)-Ti(1)-C(7)	75.90(14)
C(3)-Ti(1)-C(7)	124.86(15)
C(8)-Ti(1)-C(7)	34.91(16)
C(10)-Ti(1)-C(7)	57.62(15)
C(2)-Ti(1)-C(7)	134.11(14)
C(9)-Ti(1)-C(7)	57.19(15)
C(1)-Ti(1)-C(7)	159.97(15)
O(11)-Ti(1)-C(4)	119.41(14)
O(21)-Ti(1)-C(4)	78.89(13)
C(3)-Ti(1)-C(4)	34.56(15)
C(8)-Ti(1)-C(4)	109.07(15)
C(10)-Ti(1)-C(4)	134.02(15)
C(2)-Ti(1)-C(4)	57.79(15)
C(9)-Ti(1)-C(4)	108.08(15)
C(1)-Ti(1)-C(4)	57.49(15)
C(7)-Ti(1)-C(4)	137.85(16)
O(11)-Ti(1)-C(5)	86.95(14)
O(21)-Ti(1)-C(5)	89.59(14)
C(3)-Ti(1)-C(5)	57.46(14)
C(8)-Ti(1)-C(5)	143.43(16)
C(10)-Ti(1)-C(5)	136.77(16)
C(2)-Ti(1)-C(5)	57.45(15)
C(9)-Ti(1)-C(5)	131.64(15)
C(1)-Ti(1)-C(5)	34.55(15)
C(7)-Ti(1)-C(5)	165.45(15)

C(4)-Ti(1)-C(5)	34.50(15)
O(11)-Ti(1)-C(6)	75.95(13)
O(21)-Ti(1)-C(6)	104.26(14)
C(3)-Ti(1)-C(6)	132.02(15)
C(8)-Ti(1)-C(6)	57.08(15)
C(10)-Ti(1)-C(6)	34.88(15)
C(2)-Ti(1)-C(6)	116.51(15)
C(9)-Ti(1)-C(6)	56.79(14)
C(1)-Ti(1)-C(6)	127.45(16)
C(7)-Ti(1)-C(6)	33.78(17)
C(4)-Ti(1)-C(6)	164.53(13)
C(5)-Ti(1)-C(6)	157.84(15)
C(2)-C(1)-C(5)	108.6(4)
C(2)-C(1)-Ti(1)	72.4(2)
C(5)-C(1)-Ti(1)	73.5(2)
C(2)-C(1)-H(1)	125.7
C(5)-C(1)-H(1)	125.7
Ti(1)-C(1)-H(1)	120.1
C(1)-C(2)-C(3)	107.4(4)
C(1)-C(2)-Ti(1)	73.2(2)
C(3)-C(2)-Ti(1)	71.5(2)
C(1)-C(2)-H(2)	126.3
C(3)-C(2)-H(2)	126.3
Ti(1)-C(2)-H(2)	120.8
C(4)-C(3)-C(2)	108.7(4)
C(4)-C(3)-Ti(1)	74.5(2)
C(2)-C(3)-Ti(1)	73.3(2)
C(4)-C(3)-H(3)	125.7
C(2)-C(3)-H(3)	125.7
Ti(1)-C(3)-H(3)	118.4
C(3)-C(4)-C(5)	107.5(4)
C(3)-C(4)-Ti(1)	71.0(2)
C(5)-C(4)-Ti(1)	73.1(2)
C(3)-C(4)-H(4)	126.2
C(5)-C(4)-H(4)	126.2
Ti(1)-C(4)-H(4)	121.5
C(1)-C(5)-C(4)	107.7(4)
C(1)-C(5)-Ti(1)	71.9(2)
C(4)-C(5)-Ti(1)	72.4(2)
C(1)-C(5)-H(5)	126.1
C(4)-C(5)-H(5)	126.1
Ti(1)-C(5)-H(5)	121.3
C(7)-C(6)-C(10)	108.6(4)
C(7)-C(6)-Ti(1)	72.3(2)
C(10)-C(6)-Ti(1)	71.3(2)
C(7)-C(6)-H(6)	125.7
C(10)-C(6)-H(6)	125.7
Ti(1)-C(6)-H(6)	122.3
C(6)-C(7)-C(8)	107.8(4)
C(6)-C(7)-Ti(1)	73.9(3)
C(8)-C(7)-Ti(1)	71.4(2)
C(6)-C(7)-H(7)	126.1
C(8)-C(7)-H(7)	126.1
Ti(1)-C(7)-H(7)	120.5
C(9)-C(8)-C(7)	107.7(4)
C(9)-C(8)-Ti(1)	73.8(2)
C(7)-C(8)-Ti(1)	73.7(2)
C(9)-C(8)-H(8)	126.1
C(7)-C(8)-H(8)	126.1
Ti(1)-C(8)-H(8)	118.3

C(8)-C(9)-C(10)	109.0(4)
C(8)-C(9)-Ti(1)	71.8(2)
C(10)-C(9)-Ti(1)	72.5(2)
C(8)-C(9)-H(9)	125.5
C(10)-C(9)-H(9)	125.5
Ti(1)-C(9)-H(9)	121.9
C(9)-C(10)-C(6)	106.8(4)
C(9)-C(10)-Ti(1)	73.1(2)
C(6)-C(10)-Ti(1)	73.8(2)
C(9)-C(10)-H(10)	126.6
C(6)-C(10)-H(10)	126.6
Ti(1)-C(10)-H(10)	118.5
S(1)-O(11)-Ti(1)	153.0(2)
O(13)-S(1)-O(12)	119.0(2)
O(13)-S(1)-O(11)	111.41(19)
O(12)-S(1)-O(11)	113.71(18)
O(13)-S(1)-C(11)	106.25(19)
O(12)-S(1)-C(11)	105.7(2)
O(11)-S(1)-C(11)	98.09(18)
F(12)-C(11)-F(11)	107.5(3)
F(12)-C(11)-C(12)	108.9(3)
F(11)-C(11)-C(12)	107.3(3)
F(12)-C(11)-S(1)	108.6(3)
F(11)-C(11)-S(1)	107.8(3)
C(12)-C(11)-S(1)	116.6(3)
F(13)-C(12)-F(14)	108.3(3)
F(13)-C(12)-C(13)	107.8(3)
F(14)-C(12)-C(13)	108.5(3)
F(13)-C(12)-C(11)	108.9(3)
F(14)-C(12)-C(11)	108.2(3)
C(13)-C(12)-C(11)	115.2(3)
F(16)-C(13)-F(15)	108.6(4)
F(16)-C(13)-C(12)	109.1(3)
F(15)-C(13)-C(12)	110.0(3)
F(16)-C(13)-C(14)	107.2(3)
F(15)-C(13)-C(14)	106.1(3)
C(12)-C(13)-C(14)	115.5(4)
F(19)-C(14)-F(17)	109.0(4)
F(19)-C(14)-F(18)	107.6(4)
F(17)-C(14)-F(18)	108.0(4)
F(19)-C(14)-C(13)	111.7(4)
F(17)-C(14)-C(13)	111.5(4)
F(18)-C(14)-C(13)	108.9(4)
O(23)-S(2)-O(22)	117.00(19)
O(23)-S(2)-O(21)	113.12(17)
O(22)-S(2)-O(21)	112.46(17)
O(23)-S(2)-C(21)	105.77(19)
O(22)-S(2)-C(21)	105.29(19)
O(21)-S(2)-C(21)	101.33(17)
S(2)-O(21)-Ti(1)	138.97(18)
F(21)-C(21)-F(22)	107.9(3)
F(21)-C(21)-C(22)	109.0(3)
F(22)-C(21)-C(22)	108.8(3)
F(21)-C(21)-S(2)	106.6(3)
F(22)-C(21)-S(2)	108.4(3)
C(22)-C(21)-S(2)	116.0(3)
F(24)-C(22)-F(23)	108.1(3)
F(24)-C(22)-C(21)	108.4(3)
F(23)-C(22)-C(21)	108.2(3)
F(24)-C(22)-C(23)	108.2(3)

F(23)-C(22)-C(23)	107.9(3)
C(21)-C(22)-C(23)	115.8(4)
F(26)-C(23)-F(25)	108.5(4)
F(26)-C(23)-C(24)	107.9(4)
F(25)-C(23)-C(24)	105.9(3)
F(26)-C(23)-C(22)	109.4(3)
F(25)-C(23)-C(22)	109.1(4)
C(24)-C(23)-C(22)	115.8(4)
F(29)-C(24)-F(27)	108.7(5)
F(29)-C(24)-F(28)	107.2(4)
F(27)-C(24)-F(28)	107.1(4)
F(29)-C(24)-C(23)	113.0(4)
F(27)-C(24)-C(23)	110.9(4)
F(28)-C(24)-C(23)	109.6(4)

Table S5. Anisotropic displacement parameters ($Å^2 x\ 10^3$) for $Cp_2Ti(PFBS)_2$. The anisotropic displacement factor exponent takes the form: $-2\pi^2[\ h^2\ a^{*2}U^{11} + ... + 2\ h\ k\ a^*\ b^*\ U^{12}\ ]$

	U^{11}	U^{22}	U^{33}	U^{23}	U^{13}	U^{12}
Ti(1)	22(1)	20(1)	28(1)	0(1)	7(1)	-1(1)
C(1)	24(2)	39(2)	27(2)	5(2)	0(2)	1(2)
C(2)	25(2)	26(2)	38(2)	-8(2)	5(2)	-11(2)
C(3)	27(2)	29(2)	33(2)	5(2)	10(2)	-7(2)
C(4)	28(2)	28(2)	35(2)	1(2)	16(2)	-4(2)
C(5)	23(2)	31(2)	41(2)	4(2)	7(2)	0(2)
C(6)	24(2)	27(2)	52(3)	2(2)	16(2)	2(2)
C(7)	17(2)	31(2)	57(3)	-13(2)	7(2)	0(2)
C(8)	33(2)	35(2)	34(2)	1(2)	8(2)	14(2)
C(9)	31(2)	22(2)	49(3)	-2(2)	12(2)	6(2)
C(10)	30(2)	29(2)	39(2)	-6(2)	11(2)	7(2)
O(11)	34(2)	27(1)	35(2)	4(1)	9(1)	1(1)
S(1)	40(1)	23(1)	27(1)	2(1)	10(1)	1(1)
O(12)	40(2)	45(2)	36(2)	6(1)	14(1)	9(1)
O(13)	63(2)	29(1)	33(2)	0(1)	11(2)	-10(2)
C(11)	36(2)	27(2)	38(2)	5(2)	10(2)	0(2)
F(11)	63(2)	22(1)	38(1)	1(1)	18(1)	-1(1)
F(12)	36(2)	57(2)	35(1)	1(1)	8(1)	8(1)
C(12)	35(2)	24(2)	35(2)	2(2)	8(2)	0(2)
F(13)	34(2)	47(2)	43(1)	-3(1)	6(1)	-1(1)
F(14)	60(2)	24(1)	39(1)	3(1)	9(1)	-4(1)
C(13)	41(3)	26(2)	35(2)	2(2)	10(2)	-6(2)
F(15)	64(2)	30(1)	39(1)	-1(1)	22(1)	2(1)
F(16)	47(2)	55(2)	38(1)	2(1)	15(1)	-13(1)
C(14)	61(4)	41(3)	32(2)	1(2)	7(2)	-14(2)
F(17)	60(2)	40(2)	43(2)	10(1)	5(1)	-4(1)
F(18)	90(3)	51(2)	29(1)	-5(1)	16(2)	-13(2)
F(19)	63(2)	61(2)	38(1)	10(1)	-6(1)	-28(2)
S(2)	35(1)	24(1)	29(1)	-1(1)	8(1)	3(1)
O(21)	33(2)	23(1)	34(1)	-3(1)	8(1)	1(1)
O(22)	54(2)	27(2)	36(2)	7(1)	11(1)	7(1)
O(23)	32(2)	34(2)	40(2)	-4(1)	12(1)	2(1)
C(21)	38(2)	28(2)	35(2)	-5(2)	15(2)	1(2)
F(21)	46(2)	26(1)	41(1)	-8(1)	10(1)	-1(1)
F(22)	34(1)	40(1)	41(1)	-3(1)	15(1)	-3(1)
C(22)	33(2)	26(2)	35(2)	-3(2)	14(2)	1(2)
F(23)	34(1)	49(2)	36(1)	2(1)	14(1)	2(1)
F(24)	51(2)	27(1)	38(1)	0(1)	6(1)	-1(1)
C(23)	39(3)	36(2)	34(2)	-7(2)	3(2)	7(2)
F(25)	63(2)	35(1)	49(2)	-4(1)	0(1)	-13(1)
F(26)	36(2)	70(2)	47(2)	-1(1)	5(1)	7(1)

C(24)	51(3)	43(2)	33(2)	-4(2)	0(2)	4(2)
F(27)	72(2)	48(2)	43(2)	6(1)	1(1)	-10(2)
F(28)	61(2)	60(2)	38(2)	-7(1)	-8(1)	2(2)
F(29)	71(2)	86(2)	36(2)	-3(1)	16(2)	18(2)

References

1. Gross, E. K. U.; Dreizler, R. M.; North Atlantic Treaty Organization. Scientific Affairs, D., *Density Functional Theory*. Springer: 1995.

2. Baroni, S.; Gironcoli, S. d.; Corso, A. D.; Giannozzi, P. http://www.pwscf.org

3. Vanderbilt, D. *Phys. Rev. B* **1990**, *41*, 7892.

4. Langreth, D. C.; Perdew, J. P. *Phys. Rev. B* **1980**, *21*, 5469.

5. Ismail-Beigi, S.; Louie, S. G. *Phys. Rev. Lett.* **2003**, *90*, 076401.

6. Evans, D. F. *J. Chem. Soc.* **1959**, 2003.

7. An, D. L.; Peng, Z. H.; Orita, A.; Kurita, A.; Man-e, S.; Ohkubo, K.; Li, X. S.; Fukuzumi, S.; Otera, J. *Chem. Eur. J.* **2006**, *12*, 1642.

8. Qiu, R. H.; Zhang, G. P.; Xu, X. H.; Zou, K. B.; Shao, L. L.; Fang, D. W.; Li, Y. H.; Orita, A.; Saijo, R.; Mineyama, H.; Suenobu, T.; Fukuzumi, S.; An, D. L.; Otera, J. *J. Organomet. Chem.* **2009**, *694*, 1524.

9. Sheldrick, G. M. *Acta Crystallogr., Sect. A: Found. Crystallogr.* **2008**, *A64*, 112.

10. Clearfield, A.; Warner, D. K.; Saldarriaga-Molina, C. H.; Ropal, R.; Bernal, I. *Can. J. Chem.* **1975**, *53*, 1622.

11. Kalirai, B. S.; Foulon, J. D.; Hamor, T. A.; Jones, C. J.; Beer, P. D.; Fricker, S. P. *Polyhedron* **1991**, *10*, 1847.

12. Curtis, M. D.; Thanedar, S.; Butler, W. M. *Organometallics* **1984**, *3*, 1855.

13. Lacroix, F.; Plecnik, C. E.; Liu, S. M.; Liu, F. C.; Meyers, E. A.; Shore, S. G. *J. Organomet. Chem.* **2003**, *687*, 69.

14. Farrugia, L. J. *J. Appl. Crystallogr.* **1997**, *30*, 565.